Društvo za tehniku zavarivanja Slavonski Brod

12. Međunarodno znanstveno-stručno savjetovanje SBZ 2023

„STROJARSKE TEHNOLOGIJE U IZRADI ZAVARENIH KONSTRUKCIJA I PROIZVODA, SBZ 2023."
Slavonski Brod, 26. i 27. 04. 2023. i Požega 28. 04. 2023.

INFLUENCE OF HIGH HEAT INPUT OF D-ARC WELDING PROCESS ON THE WELD PROPERTIES FROM S355 STEEL

Tomaž Vuherer[1,*], Ivica Garašić[2], Marjan Golob[3], Mersida Manjgo[4], Darko Bajić[5], Gorazd Lojen[1]

[1]University of Maribor, Faculty of Mechanical Engineering, Maribor, Slovenia
[2]University of Zagreb, Faculty of Mechanical Engineering and Naval Architecture, Zagreb, Croatia
[3]University of Maribor, Faculty of Mechanical Electrical Engineering and Computer Science, Maribor, Slovenia
[4]"Džemal Bijedić" University of Mostar, Faculty of Mechanical Engineering 5University of Podgorica, Faculty of Mechanical Engineering

[*] Corresponding Author. E-mail: tomaz.vuherer@um.si

Abstract

The properties of welds welded by the new D-Arc ("buried arc") welding process were investigated on S355 J2 +N structural steels. Measurements of welding voltage and current show a stable welding process with the current changing from 320 A to 610 A. Microstructural analysis and hardness measurements were performed. The investigation is devoted to Charpy impact toughness, which can be one of the most critical mechanical properties in welded joints made of such steels when welding is performed with high heat input during welding. The results of the investigation with the instrumented Charpy pendulum showed that high productivity welding with the new D-Arc welding process can meet the Charpy impact energy requirements for the welded joint at -20°C.

Keywords: Weld, D-Arc process, buried arc, tensile test, hardness, Instrumented Charpy test, toughness

1. Introduction

In general, many different methods for joining heavy plates are mentioned in the literature. The most commonly used are: Submerged arc welding, GMAW with cold wire, narrow gap welding, etc. All these methods are used to achieve better deposition rate, better productivity and higher cost efficiency

in welding [1]. Welding with the so-called buried arc is also a possibility for welding heavy plates. The term "buried arc" usually refers to a type of GMAW transfer in which the arc length is relatively short and the wire end is essentially buried in the molten metal. This stage results from a relatively low arc voltage that shortens the arc length. This is similar to globular transfer with the wire end is embedded in the molten metal. Very high deposition rates are possible with this welding process. In practise, the welding arc is generated in a position above the molten metal. In this type of arc, only the top of the molten metal is heated, which is the main reason for the limited penetration depth. To weld thick materials, the groove must be prepared, and multilayer welding is usually used to join thick materials with GMAW welding. In buried arc, the welding arc is formed under the surface of the molten metal. Since the heat input from the arc occurs at a deeper level of the base material than with classical arc, a very deep penetration can be achieved. The main difference between classical welding and welding with "Buried Arc" is shown in Figure 1.

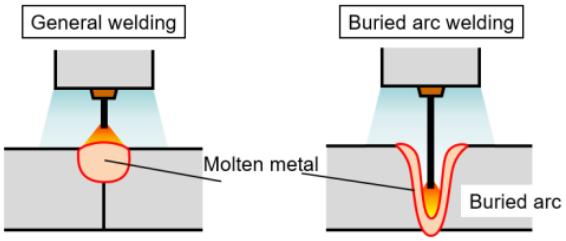

Figure 1: The difference between classical welding and welding with "Buried Arc".

The buried arc's ability to penetrate deep below the surface is utilised by the newly introduced D-Arc system developed by DAIHEN Corporation [2].
Compared to classical multilayer welding processes with high currents in thick materials, the D-Arc welding process requires shorter welding time and simpler weld preparation with smaller opening angle. Therefore, the welding wire consumption is lower due to the smaller opening angle of the groove. The main difference in weld preparation between high current welding and welding with the D-Arc process is shown in Figure 2.

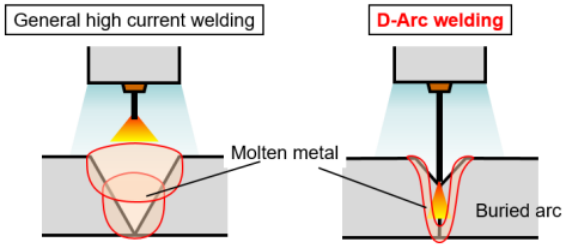

Figure 2: The difference in groove preparation between classical high current welding and D-Arc welding.

In multilayer welding processes, more filler metal is needed in the groove. This means that the cost of a filler metal is higher. When many weld passes are placed in a wide weld groove, a higher volume of molten material can be achieved with less heat input, resulting in a narrower HAZ. This type of welding has a positive effect on the microstructure and toughness of the weld and HAZ, but on the other hand, the sum of these individual local heat inputs can lead to higher residual stresses and greater deformation of the weld.
In this paper, the above mentioned advantages of the newly developed D ARC process are investigated. Special attention is devoted to the high heat input during welding on the properties of the welded joint such as tensile strength, hardness, toughness and microstructural analysis.

2. Base and filler material

Sheets of structural steel S355J2N+N were used as a base material. Their thickness was 20 mm. The steel was in the normalised state before welding. The chemical composition of the steel and its mechanical properties are given in Tables 1 and 2.

Table 1: Chemical composition of base material

C	Si	Mn	P	S	N	Cu
0.17	0.24	1.25	0.016	0.006	0.008	0.23
Cr	Ni	Mo	Al	V	Ti	Nb
0.06	0.1	0.11	0.032	0.005	0.025	0.033

Table 2: Mechanical properties of the base material

$R_{p0.2}$ [MPa]	R_m [MPa]	A_5 [%]	A_v [J]	T [°C]
429	580	21	58	-20

The filler metal used in this study was a welding wire VAC 60 with a diameter of 1.6 mm, classified as G42 5M/C G3Si1 according to the ISO 14341-A standard. The chemical composition of the wire is shown in Table 3 and its mechanical properties are shown in Table 4.

Table 3: Chemical composition of the G3Si1 filler material

C	Si	Mn	P	S
0.08	0.90	1.50	<0.025	<0.025

Table 4: Mechanical properties of filler material (by producer)

$R_{p0.2}$ [MPa]	R_m [MPa]	A_5 [%]	A_v [J]	T [°C]
> 420	500 - 640	20	47	-50

3. Experimental proceture

Before welding, a half V-shaped groove was milled and prepared for welding. The geometry of the weld (steel plates) before welding is shown in Figure 3.

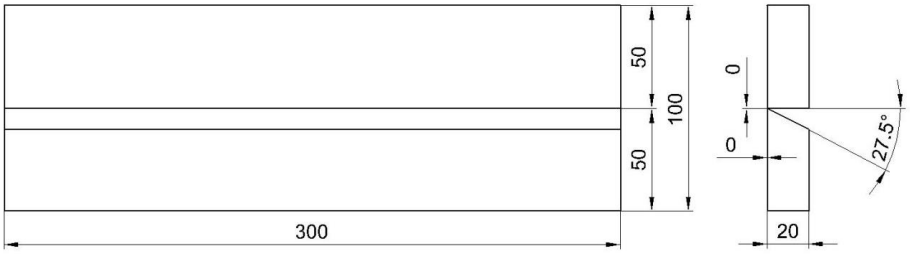

Figure 3: Geometry of the welded joint.

Welding was performed by the new D-Arc welding process using only one layer on the 20 mm thick material, by using semi-V bevel preparation with angle of 27.5°. Parameters of welding with D-Arc process are listed in table 5.

Since the process is quite new, its efficiency is still under investigation. Therefore, the efficiency 0.8 of the MAG process (Q = 35.1 kJ/cm) was used to calculate the heat input. If the efficiency 1 of the SAW process is taken into account, the heat input is 43.9 kJ/cm. The actual value of the efficiency of the D ARC process is probably between the above values, because the buried arc is under the surface of the molten metal. The photo of the welding equipment and welding setup taken immediately after welding is shown in Figure 4 and Figure 5.

Table 5: Parameters of the D-Arc welding

Welding current	Welding voltage	Welding speed	Wire feed speed	Bevel preparation		Welding gun	Heat input
I (A)	U (V)	v_v (cm/min)	v_{wire} (m/min)	Type Semi-V	Opening angle (°)	inclination angle	Q (kJ/cm)
500A	39.5	27	11.4	no gap	27.5	neutral	35.1

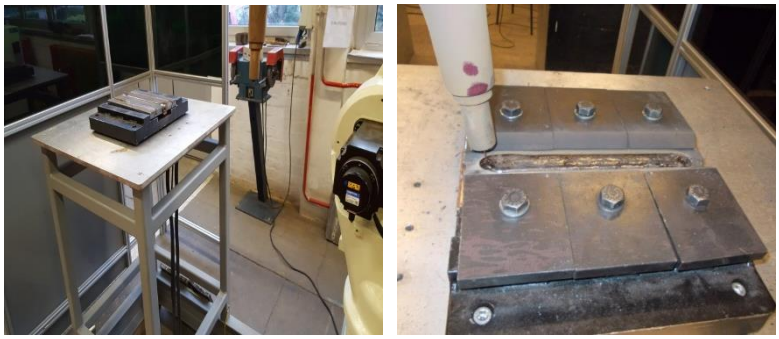

Figure 4: The photo of the weld setup taken immediately after welding [4].

Figure 5: The photo of OTC FD-V20S robot and welding sources M500D used at welding [4]

4. Results

4.1 Measuring of voltage and current signals during welding

During welding, the magnitude and shape of the voltage was measured at the clamps between the mass and the tube pack of the welding gun. The magnitude and shape of the welding current was measured with current clamps on the tube pack. Weld voltage and current were recorded synchronously during welding using an NI63XX DAQ card. The LabView software package was used for the acquisition. During welding, a signal of 1 second duration was repeatedly recorded at an acquisition rate of 1 000 000 data per second. Both signals are shown in Figure 6. The extracted signals of welding voltage and welding current in the period from 0.750 to 0.802 s are presented in Figure 7a. After filtering the extracted signals with a 5-kHz low-pass filter. The measurements of the welding voltage and current show a stable welding process where the current was changed from 320 A to 610 A with a period of 90-95 millisecond. The filtered signals are shown in Figure 7b.

a. U_mean = 39.5 V

b. I_mean = 493.67 A

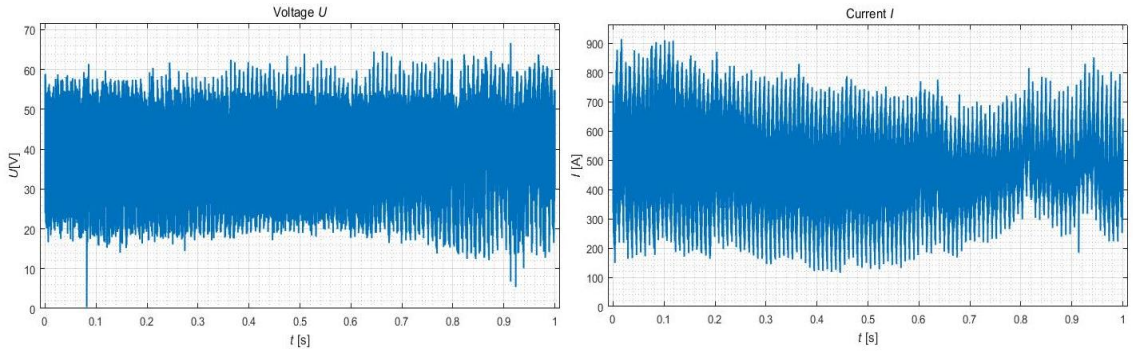

Figure 6: Welding voltage and current signals (duration 1 s)

a. U_rms = 40.1 V, I_rms = 501.8 A

b. Ulp_rms = 38.0 V, Ilp_rms = 484.3 A

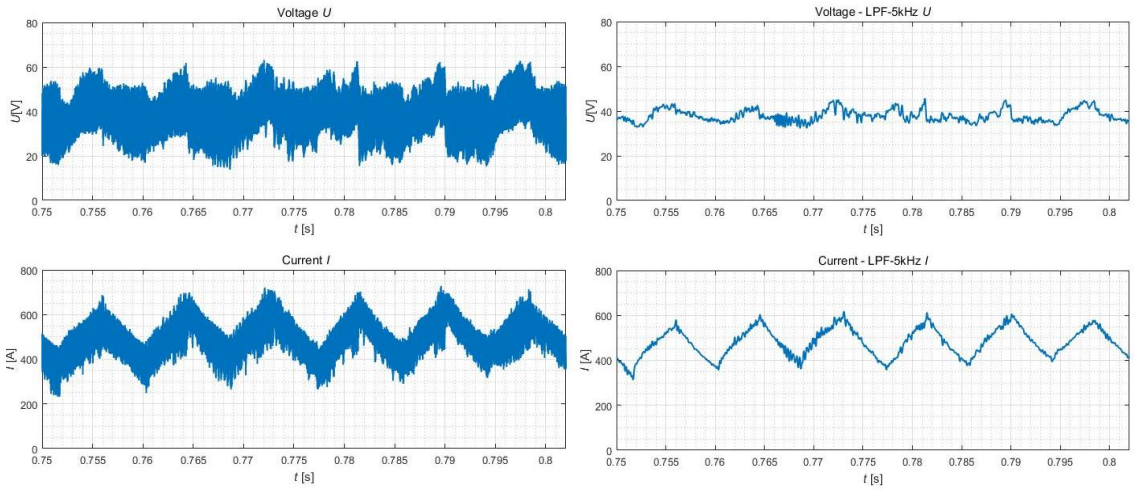

Figure 7*:* Welding voltage and current signals interval 0.75 to 0.80 s; (a) non-filtered signal, (b) filtered signal with low pass filter (LPF 5 kHz)

During D-Arc welding, two different transfer of the filler material in the arc occur when the welding current changes its value from the lower values to the upper values. Therefore, D-Arc welding process requires cyclic control for 2 modes of weld transfer. Figure 8a shows the D-Arc welding process in cross-section, while Figure 8b shows two different modes of weld transfer.

a. 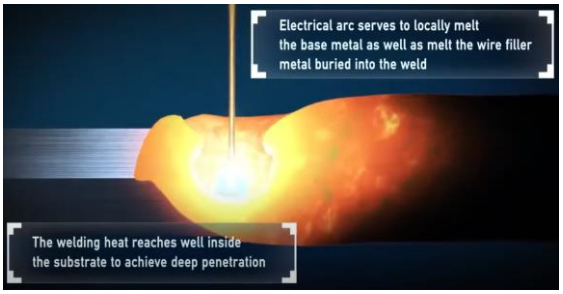

b. 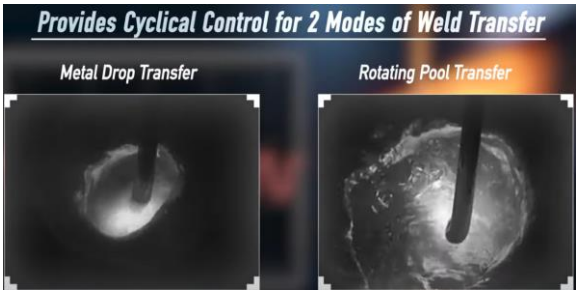

Figure 8*:* Details of D-Arc welding process; (a) Cross section of the D-Arc process, (b) cyclical control for 2 modes of weld transfer (metals drop transfer and rotating pool transfer)

Metals drop transfer, which provides heat transfer to the base material bottom for deep penetration, occurs at lower values of the welding current (Figure 9a). Rotating pool transfer, which provides a stirring action to establish and maintain the welding puddle, occurred at higher values of current (Figure 9b).

a. 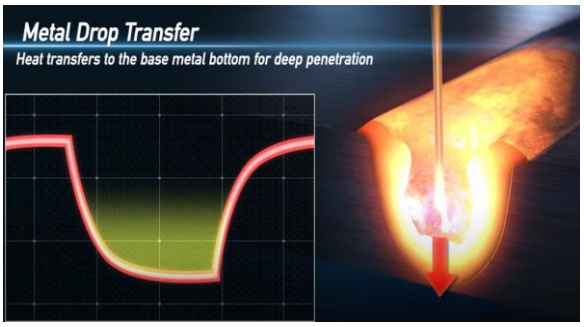

b. 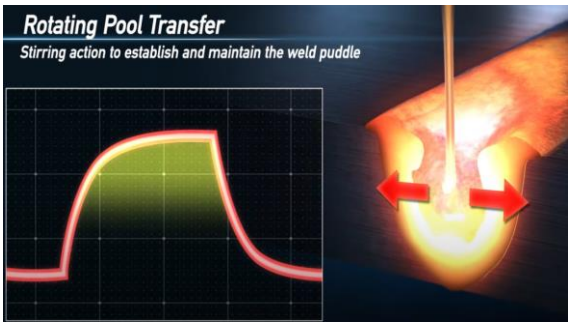

Figure 9: Cyclical control for 2 modes of weld transfer; (a) metals drop transfer at lower values of the current and (b) rotating pool transfer at higher values of current

4.2 Microstructure

The macrosections for macro- and microstructural analysis were extracted from the weld after welding. The macrosection of the weld is shown in Figure 10.

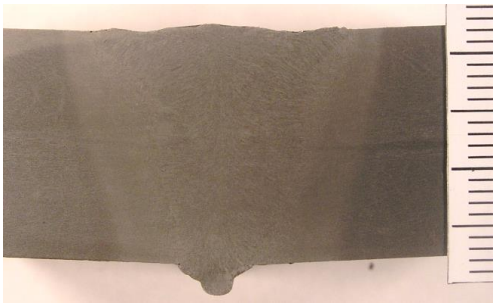

Figure 10: Macrosection of the weld joint

The results of the microstructure analysis of the base material and the CG HAZ as well as the weld metal are shown in Figure 11. An optical microscope with different magnifications was used for the microstructure analysis.

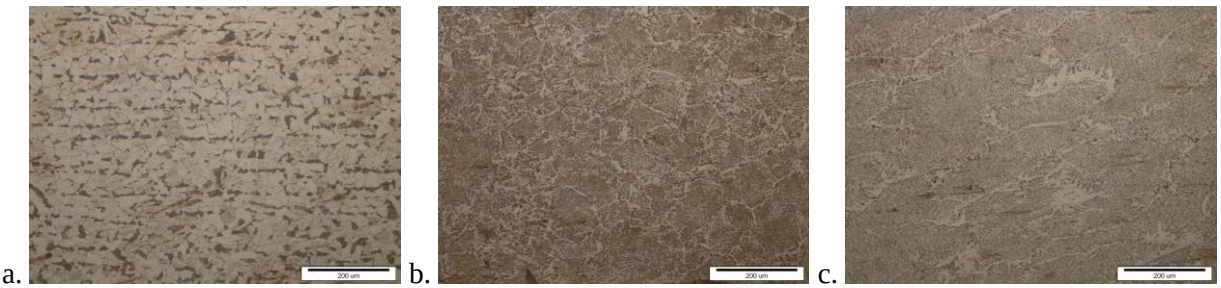

Figure 12: Microstructure of base material, coarse-grained grain heat-affected zone and weld metal

The microstructure of the base material is shown in Figure 11a. The microstructure consists of ferrite-pearlite that is normalised and has an average grain size of about 35 µm. The coarse-grained HAZ is shown in Figure 11b. This region of the HAZ was heated to above 1100 °C during heating, but was not melted. First, the grains transformed into austenite when the AC3 temperature was reached, and second, they started to grow due to the high temperature above 1100 °C. Upon cooling, they transformed into coarse-grained bainite when the Ar3 temperature was reached. The microstructure of the grains is predominantly bainite and the grain boundary structure is ferrite. The average size of the grains is about 120 µm. Figure 11c shows the microstructure of the weld metal that started to form at the fusion line with large cellular grains. The cellular grains changed from epitaxial growth at the fusion line to competitive growth and formed columnar dendritic grains in the region of the weld metal towards the centre of the weld.

4.3 Tensile tests

Cylindrical tensile specimens were machined from the base material in the transverse direction of rolling and from the weld metal in the direction of welding. The geometry of the tensile specimens is shown in Figure 13.

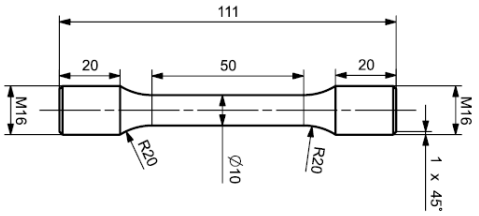

Figure 13: Geometry of the tensile specimens

Tensile tests were performed according to the standard EN ISO 6892 method B at room temperature. Table 6 contains the results of the tensile tests on the base material and the weld metal, in which the modulus of elasticity and the contraction were also measured, while Figure 14 shows the s-e diagrams for the base material and the weld metal.

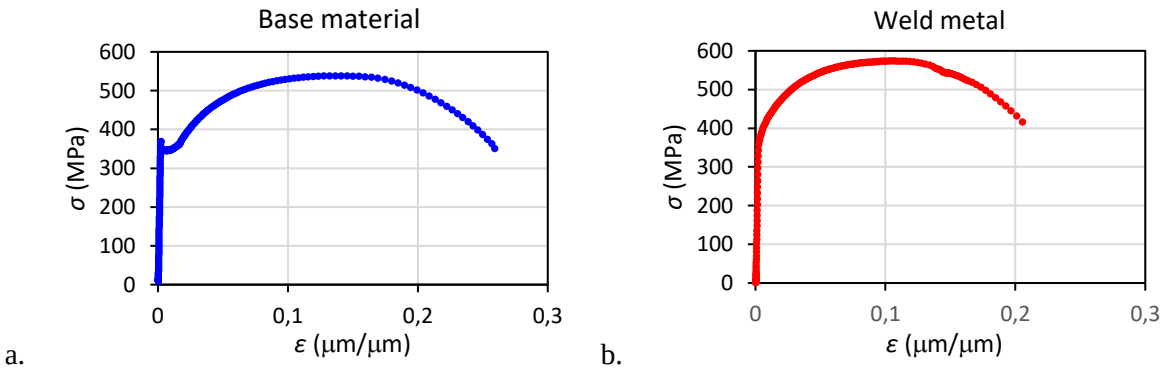

Figure 14: Results of tensile tests ($\sigma - \varepsilon$ diagram); (a) base material, (b) weld Metal

Table 6: Results of tensile tests

Mat.	$R_{p0.2}$ [MPa]	R_m [MPa]	A [%]	Z [%]	E [MPa]
BM	367	538	25.9	74	198869
WM	367	574	20.5	62	192793

4.4 Hardness measurements

The results of the Vickers hardness measurements with 98.1 N loading are shown in Figure 15, where Figure 15a shows the lines of Vickers hardness measurement points in the face and root areas of the weld 2 mm from the surface. Figure 15b shows the results of the measurements in the face region of the weld, while Figure 15c shows the results of the measurements in the root region of the weld. It can be concluded that the weld metal has a higher hardness compared to the base metal. In the HAZ, the hardness level is not too high due to the high heat input during welding.

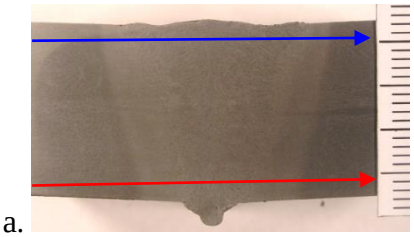

Figure 15*:* Results of hardness measurement; (a) lines of measurements, (b) face, (c) root

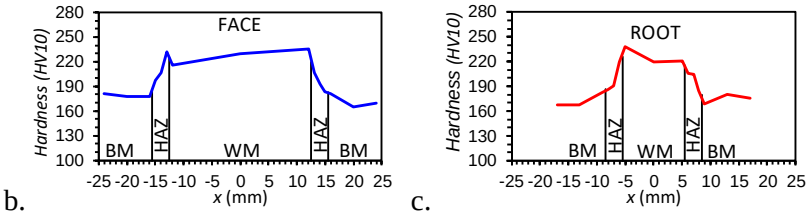

b. c.

Figure 15*:* Results of hardness measurement; (a) lines of measurements, (b) face, (c) root *(continuation)*

4.5 Instrumented Charpy tests

Charpy specimens were machined from the weld joint. The specimens were taken from different regions of the weld joint. These regions are: weld metal, fusion line and CG HAZ. All specimens were taken out from the depth 2 mm under the plate surface. Instrumented Charpy impact tests were carried out on RPK300 Amsler Charpy pendulum at two different temperatures (+20°and -20°C). During the tests force versus time diagrams were recorded and the results are presented in Table 7 and Figure 16.

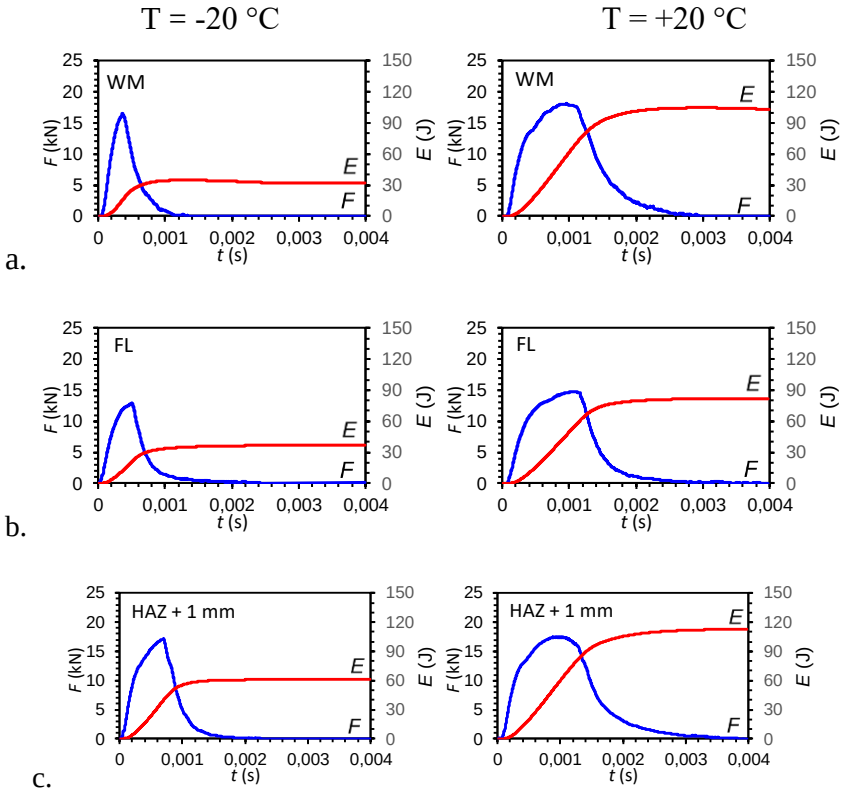

a.

b.

c.

Figure 16*:* Results instrumented Charpy test at temperatures -20 °C and +20 °C; (a) weld metal, (b) fusion line and (c) CG HAZ

The instrumented Charpy test enables to split the total energy (Av = Et) into the energy for initiation (Ei) and the energy for propagation (Ep) [3,4]. Results are shown in Table 7.

Table 7: Results of instrumented Charpy tests at temperatures -20 °C and +20 °C.

	x (mm)	T (°C)	$A_v = E_t$ (J)	E_i (J)	E_p (J)
Weld metal	0	+20	103.1	57.5	45.6
Fusin line	12	+20	82.1	46.5	35.5
CG HAZ (HAZ-1 mm)	13	+20	112.7	55.1	57.5
Weld metal	0	-20	31.9	15.6	16.3
Fusin line	12	-20	36.5	20.9	15.6
CG HAZ (HAZ-1 mm)	13	-20	60.7	40.1	20.6

The Charpy impact energy is 103 J in the weld metal at room temperature (+20°C), which is a satisfactorily high impact energy for the weld metal at high heat input (35.1 kJ/cm). Fracture analysis shows a fairly ductile surface with sheer lips on both sides of the fracture surface, and lateral expansion is high. At the fusion line, the Charpy impact energy is lowest, measured over the entire weld at +20°C. Recorded F-t diagram shows a similar shape to the weld metal, but the maximum force for fracture of the Charpy specimen is lower. The fracture surface still reflects a not so ductile fracture; therefore, the shear lips are smaller than in the weld metal, which means that a rather high lateral expansion is seen in both fracture surfaces of the specimen taken from the fusion line. The Charpy impact energy is above 110 J in all specimens taken from the CG HAZ. The force-time diagram recorded with the instrumented Charpy pendulum shows ductile fracture which is reflected in the fracture surfaces. The shear lips are large and the lateral expansion is enormous.
Charpy impact energy is lower at -20°C in all areas of the weld than at +20°C in the same areas, and shear lips and Charpy lateral expansion are also lower. The lowest Charpy impact energy is measured in the weld metal and in the fusion zone, where the microstructure with large crystal grains is the least favourable. There is a small difference in the shape of the F-t diagrams and the E-t diagrams. The area under the curve is almost identical in both diagrams. However, the energy for initiation is higher at the fusion line than in the weld metal, but the energy for propagation is lower in the fusion line. This means that even a slightly lower measured total energy in the weld metal results in a more ductile surface that is not as brittle as the sample taken from the fusion line. The Charpy specimen suddenly fractured when the force reached the maximum value. Therefore, the fracture surface at the fusion

line reflects a more brittle surface. In both cases, the Charpy impact energy is high enough to satisfy the EN ISO 15608 standard requirement of 27 J for welds on structural steels of this type.

5. Discusion

Hardness measurements reveal that the weld metal has a higher hardness compared to the base metal. In the HAZ, the hardness level is not too high due to the high heat input during welding.
The microstructure of the base material is normalised ferrite-pearlite with an average grain size of about 35 µm. The coarse-grained HAZ is predominantly bainite, and the grain boundary structure is ferritic. The average size of the grains is about 120 µm. At the fusion line, the cellular grains changed from epitaxial growth to competitive growth and formed columnar dendritic grains in the weld metal region toward the centre of the weld. Big grains in CG HAZ and big dendrites grains in the weld metal are the result of high heat input during D-Arc welding, where these areas are exposed to high temperatures for extended periods of time. This has a significant effect on the total impact energy, the energy for initiation and the energy for propagation in Charpy tests and material toughness. Table 7 shows the total and split energy for initiation and energy for propagation at -20 °C and +20 °C. There are some differences in results in Table 7. The total energy is higher at +20 °C which is normal since the test temperature is higher and the Charpy impact energy values higer. Second, the energy for initiation by the weld metal, fusion line, and CG HAZ remains almost constant, which is expected since all areas have high total energy and all fractured surfaces are mostly ductile. Compared to the results of the instrumented Charpy tests at -20°C, the energy for initiation is not the same because the total energy in the weld metal and the fusion line is too low. The energy for initiation in HAZ reaches the same energy at -20°C as at +20°C because the total energy in these areas is high enough. Both tests at +20°C and -20°C point to the weakest point of the weld joint, which in this joint is obviously the fusion line. The microstructure is the worst with the big grains on the HAZ side of HAZ and big epitaxial crystals on the weld metal side.

6. Conclusion

Measurements of the welding voltage and current on the D-Arc show a stable welding process where the current was changed from 320 A to 610 A with a period of 90 - 95 ms.
The properties of welds welded by the high-productivity D-Arc welding process (with "Buried Arc") were studied on S355 J2 +N structural steels welded with high heat input. Microstructure analysis revealed big grains in the coarse-grained HAZ, where the average grain size is about 120 µm, compared to the base material, which is 35 µm.
Both tests at +20°C and -20°C indicate the weakest point of the weld joint, which is obviously the fusion line. There the microstructure is most unfavourable with the big grains on the HAZ side and big epitaxial crystals on the weld metal side.
In both cases, the Charpy impact energy is high enough to meet the standard 27 J requirement for welds on structural steels of this type.

7. References

[1] Bajić B., Elektrolučno zavarivanje u zaštiti inertnog i aktivnog gasa MIG-MAG: tehnološke I metalurške osnove.

[2] Baba Hayato et al: Single pass full penetration joining for heavy plate steel using high current GMA process (D-Arc); *Zbornik dneva varilne tehnike 2017*.

[3] Vuherer T., Garašić I., Kastelic P., Properties od Butt-weld join welded by new D-Arc process; Doc.XII-2373-18 /212-1537-18 /IV-1374-18, *The Welding Institute group XII and IV annual meeting, Lendava 2019*

[4] Vuherer T., Dunđer M., Milović L., Zrilić M., Samardžić, I. Microstructural investigation of the heat-affected zone of simulated welded joint of P91 steel. *Metalurgija, 2013,* vol. 52, issue. 3, pp. 317-320.